Journal of Optoelectronics and Advanced Materials Vol. 6, No. 3, September 2004, p. 875 - 882

CHALCOGENIDE THIN FILMS DEPOSITED BY RADIO-FREQUENCY SPUTTERING

V. Balan, C. Vigreux*, A. Pradel

Laboratoire de Physico-chimie de la Matière Condensée, UMR 5617,
Université Montpellier II, Place Eugène Bataillon, 34095 Montpellier cedex 5, France

Several properties of chalcogenide glasses make these materials attractive candidates for integrated optics. These properties include infrared transparency, high refractive index, photosensitivity, low phonon energy and ease in preparation of thin film. We report on the radiofrequency sputtering deposition of thin columnar films of chalcogenide glasses ($Ge_{33}As_{12}Se_{55}$ and $Ge_{28}Sb_{12}Se_{60}$) and on the influence of their thickness and morphology on their optical characteristics (optical band gap and refractive index). It is shown that the higher the thickness, the larger the gathering of the columns in clusters, leading to an increase in the porosity (from 18 % for 0.2 μm thick films to 33 % for 5 μm thick ones), and to a decrease in the optical band gap and refractive index (about 10 %).

(Received July 23, 2004; accepted August 27, 2004)

Keywords: Chalcogenide thin films, Sputtering, Morphology, Optical properties

1. Introduction

Due to their transparency in the infrared, their high refractive index, their well-known photosensitivity properties and their ease in preparation of thin film, interest in chalcogenide glasses for integrated optics and technological applications related to detection in the IR spectral domain (environmental metrology [1-3] and spatial interferometry [4,5] for example) has been growing over the past few years. Moreover, because of their very low phonon energies ranging between 200 and 470 cm^{-1} depending on the composition, chalcogenide glasses are also good potential candidates for efficient rare-earth doped optical amplifiers and emitters [6].

Integrated optical components require thin films of large size, desired thickness and composition, good homogeneity and adherence to the substrate and controlled optical properties. Many techniques have been proposed to deposit chalcogenide glasses, undoped or doped by rare earth ions: thermal evaporation [7-9], pulsed laser deposition [6], CVD [10-12], spin coating [13-16], RF sputtering [17,18]. It is known that the optical properties of thin films are not always the same as those of corresponding bulk glasses, due to the deposition processes which organise glasses in different ways. Some recent works deal with the influence of the film composition on the refractive index [19,20], but none deals with the influence of the morphology on the optical properties.

The present work deals with the characterisation of $Ge_{33}As_{12}Se_{55}$ and $Ge_{28}Sb_{12}Se_{60}$ chalcogenide thin films. The films are good candidates for the realisation of opto-chemical sensors [2]: in addition to their large transparency domain and high refractive index, the $Ge_{33}As_{12}Se_{55}$ and $Ge_{28}Sb_{12}Se_{60}$ compositions were chosen for their good chemical and thermal stabilities (Tg = 362 °C and 278 °C, respectively). In this work, particular attention is paid to the study of the homogeneity of the films deposited by radio-frequency sputtering and the influence of their morphology on the optical properties (optical band gap and refractive index).

* Corresponding author: cvigreux@lpmc.univ-montp2.fr

2. Experimental procedures

The $Ge_{33}As_{12}Se_{55}$ and $Ge_{28}Sb_{12}Se_{60}$ films were deposited by RF-sputtering from 5 cm-diameter IG2 and IG5 VITRON commercial targets, respectively, using an Alcatel Dion 300 device equipped with a PFG 300 RF Huttinger, 13.56 MHz, 300 W generator. Before the deposition, the chamber was evacuated down to approximately 10^{-4} Pa to avoid ambient contamination. An operating argon pressure comprised between 1 and 10 Pa was used. A low RF power, 25 W, was imposed because of the dielectric character of the chalcogenide glasses [21]. As an example, the deposition rate under an argon pressure of 5 Pa was 0.25 $\mu m.h^{-1}$. Microscope slides (7.6×2.6 cm^2) were mainly used as substrates. Before being introduced in the vacuum chamber, they were cleaned with a commercial DECON detergent in an ultrasonic bath, rinsed in alcohol and dried with dry air. In order to check the influence of the substrate on the morphology of the layers, we also deposited few layers on silicon substrates. These were cleaned one minute in HF (40%) before being dried with dry air. The substrate holder was neither rotated nor heated, but cooled down by water circulation. The targets were polished systematically previous to deposition in order to ensure reproducibility.

The adherence of the films on the substrates was checked by the classical adhesive tape test. The thickness was estimated by profilometry (using a DEKTAK 3 Veeco). The film surface aspect and roughness were inspected using a DIGITAL INSTRUMENTS D3100 Atomic Force Microscopy. The film structure was investigated thanks to an HITACHI Scanning Electron Microscopy. Chemical composition was estimated using a CAMECA 100SX Wavelength Dispersive Spectrometer. The optical transmittance was recorded with an UV-visible spectrophotometer (CARY 50 from VARIAN). The transmittance spectra were used to obtain the band gap energy (E_g) of the films and to estimate the Urbach parameter (E_e) which is a characteristic of the disorder. Refractive indices were estimated by ellipsometry (using a UVISEL HR46 from JOBIN-YVON).

3. Results

Thickness measured at different points of the deposited films was shown to be maximum at the centre and to decrease as the point moves away from it (Fig. 1), following the Knudsen's cosinusoidal law (1):

$$d/d_0 = 1/(1+(l/h)^2)^2 \qquad (1)$$

where d_0 is the thickness at the film centre, l the distance between the target and the substrate (i.e. 5.5 cm) and h the distance between the centre of the layer and its extremity (i.e. 3.5 cm). This is a classical result for films deposited by RF sputtering when the substrates are not rotated.

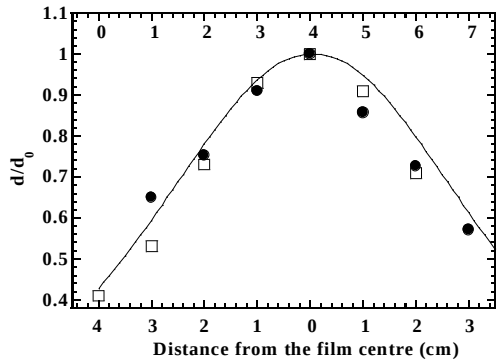

Fig. 1. Thickness versus the distance from the film centre for GeSbSe films (filled circles) and for GeAsSe films (empty squares). d_0 represents the thickness at the centre. The black line corresponds to the Knudsen's theoretical sinusoïdal variation.

Films deposited under the same conditions were characterised by the same thickness at the centre. Depending upon the deposition time, films with thickness in the range 0.05 to 5 microns were obtained.

All the films adhered to the microscope slides as verified by a simple adhesive tape test. They were amorphous whatever the chalcogenide composition.

The reproducibility in composition was checked: several films ($Ge_{28}Sb_{12}Se_{60}$ and $Ge_{33}As_{12}Se_{55}$) were prepared while maintaining the same deposition conditions. The compositions were proved to be reproducible even though they were different from those of the corresponding targets. The actual compositions of the films were $Ge_{26\pm0.7}Sb_{12,2\pm0,7}Se_{61,8\pm0,6}$ and $Ge_{29\pm0,8}As_{12,2\pm0,4}Se_{58,3\pm0,7}$. They will be referred as GeSbSe and GeAsSe, respectively.

The compositions were shown to be independent of the film thickness, with variations in composition lower than 2% when the thickness was varied from 0.05 to 5 microns.

3.1. Morphological properties

Fig. 2a and Fig. 2b show AFM images of two 2 µm-thick GeAsSe films deposited under a 5 Pa argon pressure on a microscope slide and on a silicon substrate, respectively.

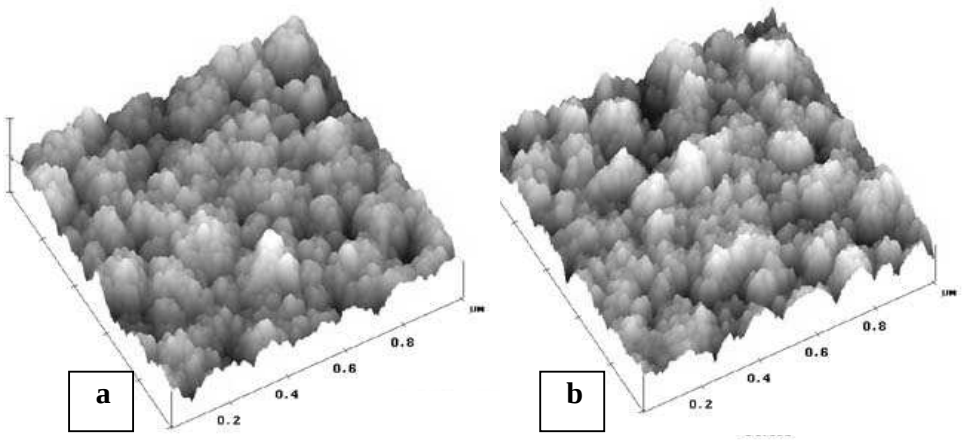

Fig. 2. AFM images of two 4-µm thick GeAsSe films deposited simultaneously under a 5 Pa argon pressure on: a) a microscope slide; b) a silicon substrate.

A columnar structure can be observed, whatever the substrate. The average column size and the root mean square (rms) roughness estimated from AFM images measured over an area of 1 µm × 1 µm were appreciably the same for the two films, that is to say about 20 nanometers and 6.5 nanometers, respectively. It is to be noted that the roughness of the cleaned microscope slide and silicon substrates are 0.5 nm and 0.2 nm, respectively. Fig. 3 compares AFM images of 2 µm-thick GeSbSe and GeAsSe films deposited under a 5 Pa argon pressure on microscope slides. A similar structure is observed for the two compositions. Note that whatever the argon pressure used between 1 and 10 Pa, a similar columnar structure was observed whatever the composition and the substrate. Images obtained by Scanning Electron Microscopy then confirmed the column-like structure within the layers. As an example, Fig. 4a and Fig. 4b show the SEM images of the cross-sections of two 4 µm-thick GeAsSe films deposited on a microscope slide and a silicon substrate, respectively.

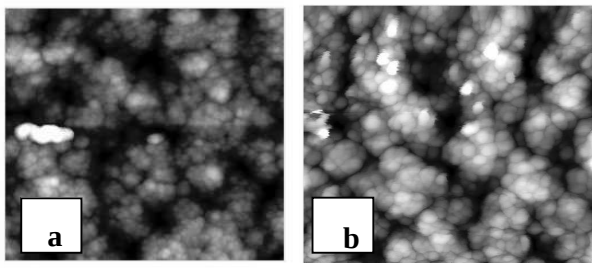

Fig. 3. AFM images of 2-µm thick chalcogenide films deposited in the same conditions of RF power and argon pressure : a) GeSbSe film: the roughness was estimated to be of 6.3 nm; b) GeAsSe film: the roughness was obtained to be of 6.9.

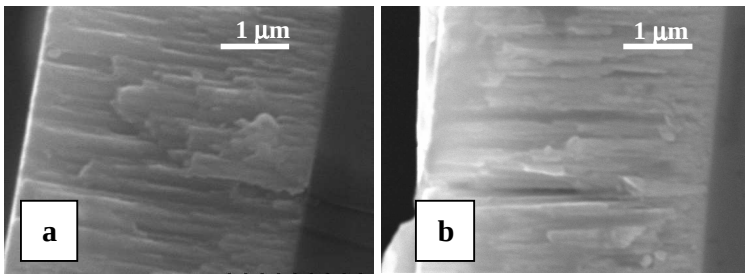

Fig. 4. SEM images of the cross-sections of two 4-µm thick GeAsSe films deposited simultaneously under a 5 Pa argon pressure on: a) a microscope slide; b) a silicon substrate.

The reproducibility of the morphological properties was checked: several films of each composition were prepared while maintaining the same deposition conditions. Only the centres of the layers were investigated. Average column size and roughness were shown to be reproducible.

The dependence of the roughness and the average column size on the thickness was then investigated. AFM images were scanned for films of different thickness. As an example, Fig.5 shows three images for GeSbSe films deposited on microscope slides under the same conditions of RF-power and argon pressure, but for different deposition times. Films with 0.2 µm (a), 1.36 µm (b) and 2.18 µm (c) in thickness were obtained. The rms values of the films were 1.1 nm, 1.9 nm and 6.3 nm, respectively. A detailed study of the AFM images revealed that the average column size was approximately the same whatever the thickness, but that the columns gathered to form clusters when the thickness increased. The clusters were approximately 250 nanometers in diameter for 4 micron-thick films. Similar results were obtained for GeAsSe films.

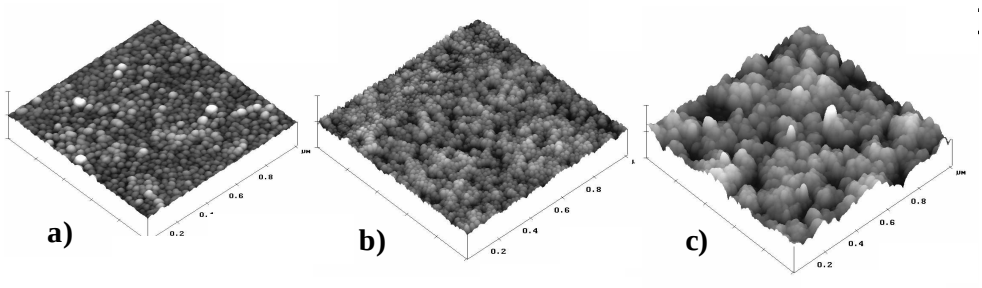

Fig. 5. AFM images of three GeSbSe thin films deposited for different times, resulting in different thickness: a) e = 0.2 µm, roughness of 1.1 nm; b) e = 1.36 µm, roughness of 1.9 nm and c) e = 2.18 µm, roughness of 6.3 nm.

The change in morphology over the surface of columnar GeSbSe and GeAsSe films deposited on microscope slides was studied by measuring the roughness at different points of the films by AFM. As an example, Fig. 6 shows the change in roughness at different points for a GeSbSe film which is 3.5 micron-thick at the centre. It can be noted that the roughness is different from one point of the film to another. It is maximum at the centre of the layer (point 0) and decreases as the point moves away from the centre. Such a variation was expected taking into account the change in the thickness at different points of the films, and the previously discussed dependence between roughness and thickness.

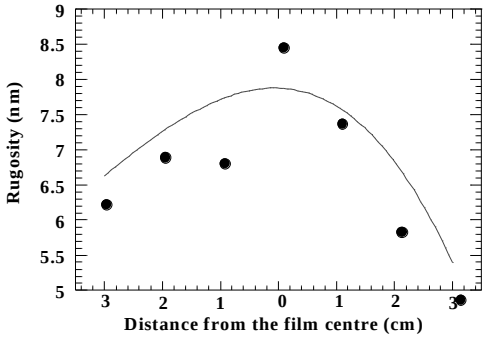

Fig. 6. Roughness measured on 7 different areas of a GeSbSe film. Point 0 corresponds to the centre of the layer.

3.2. Optical properties

The analysis of the transmission spectra allowed us to determine the band gap energy E_g and the Urbach parameter E_e using Tauc relations [22]. The band gap energy was estimated using 2, considering the high absorption (absorption coefficient $\alpha > 10^4$ cm^{-1}) part of the transmission spectra. In this region:

$$\alpha(\omega) = \beta(\hbar\omega - E_g)^2/\hbar\omega \quad (2)$$

where β is a constant which depends on the transition probability.

The E_e parameter related to the disorder in the vitreous structure was obtained from Eq.3, considering the low energy (absorption coefficient between 1 and 10^4 cm^{-1}) exponential part of the transmission spectra:

$$\alpha(\omega) = \alpha_0 \exp(\hbar\omega/E_e) \quad (3)$$

where α_0 is a constant.

The refractive indices of the GeSbSe and GeAsSe films deposited on microscope slides were obtained by ellipsometric measurements.

Firstly, the three parameters calculated at the centre of the layers were shown to be reproducible for films deposited under the same conditions (argon pressure of 5 Pa) and characterised by the same thickness.

It was then shown that the three parameters depend on the thickness of the films. Fig. 7 gives the values of the band gap energy, the E_e parameter and the refractive index at 1.55 microns, obtained for four GeSbSe films of different thickness. The energy band gap and the refractive index decrease while the Ee parameter increases with thickness.

The homogeneity of the films in terms of energy band gap and E_e parameter was then investigated for the GeSbSe and GeAsSe films. Measurements of the two parameters were done at different points of the films, as shown in Fig. 8. The band gap energy is maximum and the E_e parameter minimum at the centre of the layers (point 0 on the picture).

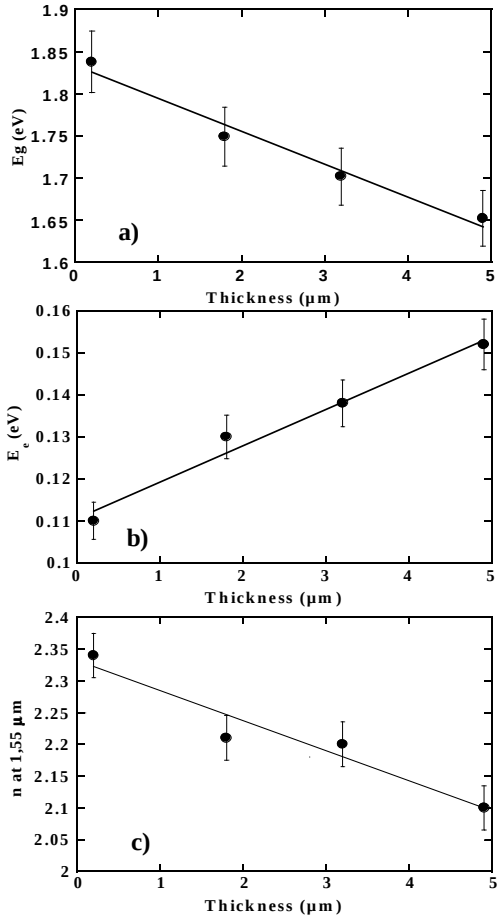

Fig. 7. a) Band gap energy E_g, b) Urbach parameter E_e and c) refractive index measured at 1.55 µm versus the GeSbSe layer thickness.

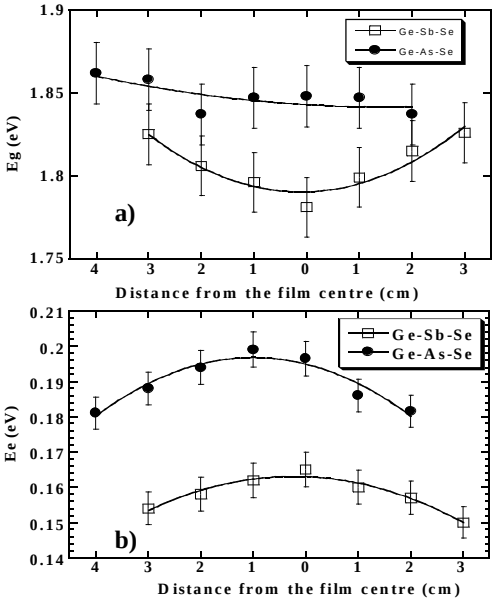

Fig. 8. a) Band gap energy E_g and b) Urbach parameter E_e of two GeSbSe and GeAsSe films versus the analysed area, point 0 corresponding to the centre of the layers.

4. Discussion

The films deposited by RF sputtering were shown not to be homogeneous in thickness, which is expected in the absence of substrate rotation.

The columnar structure of GeSbSe and GeAsSe thin films deposited by RF sputtering was highlighted by AFM measurements. The results in term of morphology were similar for the two compositions and whatever the substrate (microscope slide or silicon). The column-like structure can be explained taking into account the Thornton Zone Diagram [23], the high glass transition temperatures of the chalcogenide materials (278 and 362 °C, respectively) and the deposition conditions (pressure between 1 and 10 Pa, not-heated substrates). Indeed, three-dimensional nucleation is expected to be the dominant mechanism of film formation in the absence of substrate heating. Therefore, the film grown on the glass susbtrate most likely forms by the coalescence of islands from nucleation [24].

The columnar structure of GeSbSe and GeAsSe thin films was then shown to evolve with the thickness of the layer. For thick films, the columns of 20 nanometers in diameter gather to form clusters of approximately 250 nanometers. The consequence is an increase in roughness with the thickness of the layers.

If the composition of the films was shown to be independent of the thickness of the layers, the optical properties were shown to be intimately related to it. The refractive index of the films decreases with the thickness of the films. It can be explained by the change in the morphology of the

films with thickness. Indeed, the clusters formed by columns gathering induces an increase in empty zones and a decrease in the average refractive index is then expected. Kinoshita et al. [25] proposed an empirical relationship between the effective refractive index and the material porosity (4):

$$n = (1-p)n_s + pn_v \quad (4)$$

where n is the effective refractive index, n_v the refractive index of the empty areas, n_s the one of the material, and p the porosity.

This relationship allowed us to estimate the change in the porosity of the layers with the thickness (Fig. 9). It can be seen that porosity increases up to 33 % for a 5 microns thick film.

The decrease in the optical band gap and the increase in the E_e parameter with the thickness are intimately related to the increase in the disorder. It is clear that one can expect an increase in the disorder when the thickness of the layer increases, especially in the case of columnar films. The effect of the disorder on the E_g and E_e parameters has already been reported in thin films deposited by thermal obliqual evaporation [26-28]. The authors showed that columnar films were then obtained and their annealing led to an increase in the optical band gap and in a decrease in E_e due to densification.

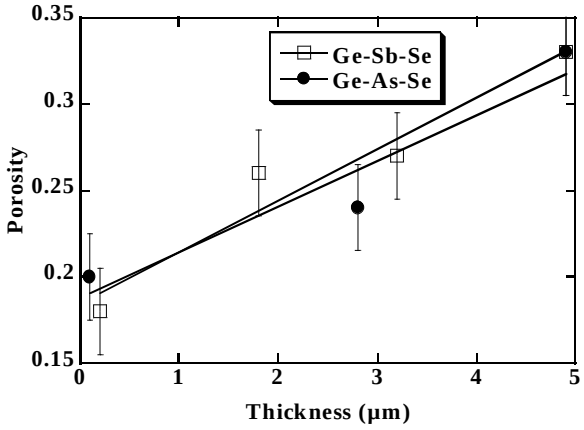

Fig. 9. Porosity of GeSbSe and GeAsSe films depending on their thickness.

5. Conclusion

The aim of the study was to evaluate the influence of the column-like structure of sputtered films on their optical properties. It was shown that in the absence of annealing, the layers are characterised by a morphology intimately related to their thickness. The larger the thickness, the larger the gathering of the columns in clusters. The size of the clusters increases up to 250 nanometers for the 5 micron-thick layers. This induces an increase in the roughness from 1.1 to 6.3 nanometers when the thickness increases from 0.2 to 2.2 microns. At the same time, the porosity of the layers increases (up to 33 % for the 5 micron thick films). The increase in the porosity leads to a decrease in the average refractive index: for thick films with 33 % porosity, the refractive index is 10 % lower than that of the thin layers with a porosity of less than 20 %.

The resulting increase in the disorder with the thickness leads to a decrease in the optical band gap E_g and an increase in the Urbach parameter E_e. Investigations on the influence of the annealing on the film morphology and optical properties are currently in progress. One can expect a densification of the layers, resulting in the disappearance of the column-like structure, an increase in E_g and a decrease in E_e.

Up to now, only an average value of the refractive index of the films has been estimated. However, a smooth evolution with depth (interesting for applications such as antireflection coating) could be expected. Therefore, investigations on the depth profile of the refractive index are to be considered.

References

[1] J. Keirsse, C. Boussard-Plédel, O. Loreal, O. Sire, B. Bureau, B. Turlin, P. Leroyer, J. Lucas, J. Non-Cryst. Solids **326/327**, 430 (2003).
[2] V. Balan, C. Vigreux, A. Pradel, A. Llobera, C. Dominguez, M. I. Alonso, M. Garriga, J. Non-Cryst. Solids **326/327**, 455 (2003).
[3] D. Le Coq, C. Boussard-Plédel, G. Fonteneau, T. Pain, B. Bureau, J. L. Adam, Materials Research Bulletin **38**(13), 1745 (2003).
[4] E. Laurent, I. Schanen, F. Malbet, G. Taillades, Astronomical Telescopes and Instrumentation, Interferometry in Optical Astronomy, Munich, Germany, March 27-31, 2000, Proc. SPIE Vol. **4006**, 1090 (2000).
[5] E. Laurent, P. Kern, I. Schanen, V. Balan, C. Vigreux, A. Pradel, R. Romestain, S. Setzu, P. Labeye, K. Perraut, P. Benech, Astronomical Telescopes and Instrumentation, Interferometry in Optical Astronomy, Hawaii, U.S.A., August 22-28, 2003, Proc. SPIE **4838**, 1344 (2003).
[6] M. Martino, A. P. Caricato, M. Fernandez, G. Leggieri, A. Jha, M. Ferrari, M. Mattarelli, Thin Solid Films **433**, 39 (2003).
[7] L. Tichy, H. Ticha, P. Nagels, R. Callaerts, R. Mertens, M. Vleck, Mater. Lett. **39**, 122 (1999).
[8] A. A. A. El-Rahman, A. M. Eid, M. Sanad, R. M. E. Ocker, J. Phys. Chem. Solids **5**(5) (1998).
[9] A. Abu-Sehly, A. Soltan, Appl. Surf. Sci. **199**, 147 (2002).
[10] E. Marquez, P. Nagels, J. M. Gonzales-Leal, A. M. Bernal-Oliva, E. Sleeckx, R. Callaerts, Vacuum **52**, 55 (1999).
[11] P. Nagels, E. Sleeckx, R. Callaerts, E. Marquez, J. M. Gonzales-Leal, A. M. Bernal-Oliva, Solid States Ionics **102**(7), 539 (1997).
[12] B. Cros, H. Camon, Y. Brocheton, J. Gonchond, A. Tissier, J. Balladore, M. Ribes, J. Phys. **50**, C5-343 (1989).
[13] S. Shtutina, M. Klebanov, V. Lyubin, S. Rosenwaks, V. Volterra, Thin Solid Films **261**, 263 (1995).
[14] K. Kase, G. C. Chern, I. Lauks, Thin Solid Films **116**, L53 (1984).
[15] G. C. Chern, I. Lauks, J. Appl. Phys. **53**(10), 6979 (1982).
[16] G. C. Chern, I. Lauks, J. Appl. Phys. **54**(5), 2701 (1983).
[17] S. Ramachandran, S. G. Bishop, Appl. Phys. Lett. **74**, 13 (1999).
[18] D. A. Turnbull, J. S. Sanghera, V. Q. Nguyen, I. D. Aggarwal, Mater. Lett. **58**(1-2), 51 (2004).
[19] J. M. Laniel, J. M. Ménard, K. Turcotte, A. Villeneuve, R. Vallée, C. Lopez, K. A. Richardson, J. Non-Crystalline Solids, **328**, 183 (2003).
[20] I. Ohlidal, D. Franta, M. Frumar, J. Jedelesky, J. Omasta, J. Optoelectron. Adv. Mater. **6**(1), 139 (2004).
[21] S. Zembutsu, S. Fukunishi, Applied Optics **18(3)**, 393 (1979).
[22] J. Tauc, R. Grigorovici, A. Vancu, Phys. Stat. Sol. **15**, 627 (1966).
[23] J. A. Thornton, J. Vac. Sci. Technol. **11**, 666 (1974).
[24] L. Mao, R. E. Benoit, J. Proscia, in: S. M. Yalisove, C. V. Thomson, D. J. Eaglesham (Eds.), Materials Research Society Symposium, Boston, U.S.A., Proc. **317**, 181 (1994).
[25] Kinoshita, M. Nishibori, in: A. Richardt, A.-M. Durand, Les interactions ions énergétiques-solides, In Fine, Paris, 357 (1997).
[26] K. Harshavardhan, S. Rajagopalan, L. K. Malhotra, K. L. Chopra, J. Appl. Phys. **54**(2), 1048 (1983).
[27] E. Marquez, A. M. Bernal-Oliva, J. M. Gonzales-Leal, R. Pietro-Alcon, R. Jimenez-Garay, J. Non-Cryst. Solids **222**, 250 (1997).
[28] K. Shimakawa, A. Ganjoo, J. Optoelectron. Adv. Mater. **3**(2), 167 (2001).